ISSN 1063-7826, Semiconductors, 2007, Vol. 41, No. 2, pp. 215–222. © Pleiades Publishing, Ltd., 2007.
Original Russian Text © V.A. Andrianov, V.P. Gor'kov, V.P. Koshelets, L.V. Filippenko, 2007, published in Fizika i Tekhnika Poluprovodnikov, 2007, Vol. 41, No. 2, pp. 221–228.

PHYSICS OF SEMICONDUCTOR DEVICES

Superconducting Tunneling-Junction Detectors of X-ray Radiation. Issues Concerning the Energy Resolution

V. A. Andrianov[a]^, V. P. Gor'kov[b]^^, V. P. Koshelets[c]^^^, and L. V. Filippenko[c]

[a]*Skobel'tsyn Research Institute of Nuclear Physics at the Moscow State University, Moscow, 119992 Russia*
^e-mail: andrva22@mail.ru

[b]*Department of Computational Mathematics and Cybernetics, Moscow State University, Moscow, 119992 Russia*
^^e-mail: v-p-gorkov@yandex.ru

[c]*Institute of Radio Engineering and Electronics, Russian Academy of Sciences, Moscow, 103907 Russia*
^^^e-mail: valery@hitech.cplire.ru

Submitted March 29, 2006; accepted for publication May 24, 2006

Abstract—The effect of the recombination- and edge-related losses of nonequilibrium quasiparticles on the energy resolution of superconducting tunneling detectors is studied. The dependence of the signal on the energy of X-ray photons is measured and the shape of instrument-related lines is studied for the Ti/Nb/Al/AlO_x/Al/Nb/NbN detectors with the Ti/Nb passive electrode. Experimental data are analyzed using the diffusion-based model of tunneling detectors.

PACS numbers: 29.40.Wk, 74.45.+c, 74.78.Fk

DOI: 10.1134/S1063782607020194

1. INTRODUCTION

At present, in Russia and abroad, there is active research in the field of development of new detectors of X-ray radiation and optical radiation on the basis of superconducting tunneling junctions (STJs) [1–3]. These detectors should have a high energy resolution and a low energy-detection threshold. Concerning the structure, the STJ detectors are composed of two superconducting electrodes separated by a thin insulator layer. Absorption of a photon in one of the STJ electrons brings about a break of the Cooper electron pairs and origination of nonequilibrium quasiparticles whose tunneling through the insulating layer forms the signal in the detector.

The number of originating quasiparticles N_0 is proportional to the radiation-photon energy E and is inversely proportional to the width of the superconducting gap Δ in the energy spectrum of the electrode where the photon is absorbed. Since the value of Δ is on the order of a millielectronvolt, the number of formed quasiparticles is larger by three orders of magnitude than in conventional semiconductor detectors. It is this circumstance that makes it possible to substantially increase the energy resolution and reduce the detection threshold in tunneling detectors. The expected energy resolution for detectors with Nb electrodes is 4–10 eV for the X-ray line at 6 keV. Unfortunately, the energy resolution is several times worse than the theoretical limit even in the best detectors produced to date.

One of the main reasons for the worsening of the resolution is the dependence of the detector signal on the coordinate that corresponds to the photon absorption (inhomogeneous broadening). The primary cloud of nonequilibrium quasiparticles occupies a relatively small region of the electrode. Further on, the quasiparticles spread over the electrode's volume owing to diffusion; it is noteworthy that the processes of tunneling (that form the detector's signal) and disappearance of quasiparticles occur simultaneously. Under disappearance is meant all processes that lead to the exclusion of quasiparticles from the tunneling process, namely, capture of quasiparticles by various traps caused by a local decrease in the width of superconducting gap Δ, processes of recombination of quasiparticles with resulting formation of the Cooper pairs, and also escape of quasiparticles to the contact regions. The detector signal is proportional to the collected charge of tunneling current. It is typically assumed that the main mechanism of inhomogeneous broadening of the line consists in the capture of nonequilibrium quasiparticles by traps formed in the vicinity of the side faces of the electrodes in the course of fabricating the tunneling junctions [4, 5]. In this case, the signal's amplitude starts to depend on the separation of the site where the photon was absorbed from the boundary.

Recombination-related losses were considered previously [6, 7]. Recombination of nonequilibrium quasiparticles with thermal quasiparticles is negligible since the temperature of the operating detector is much lower than the temperature of transition to the superconducting state. Appreciable losses can be caused only by intrinsic recombination of nonequilibrium quasiparti-

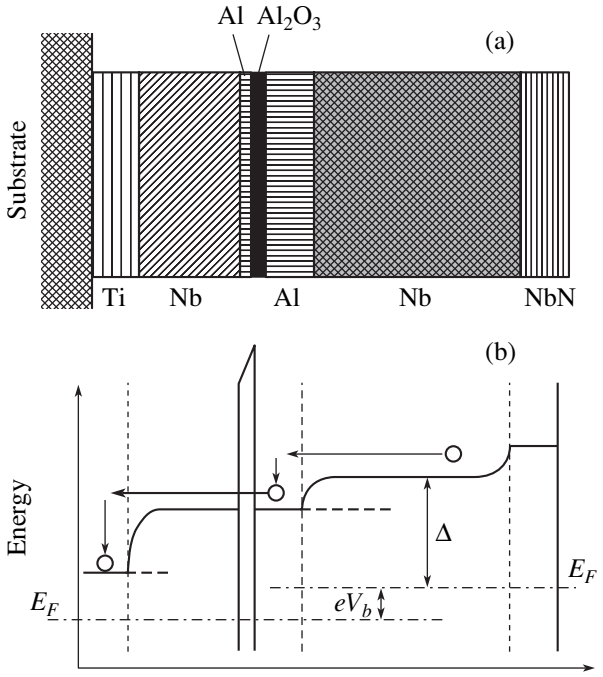

Fig. 1. The structure of a Ti/Nb/Al/AlO_x/Al/Nb/NbN tunneling detector. (a) Spatial arrangement of the layers and (b) the structure of energy levels of quasiparticles. Here, E_F is the Fermi energy, Δ is the superconducting gap, V_b is the bias voltage, and e is the elementary charge; arrows indicate the direction of motion of quasiparticles.

cles in the initial time interval, in which case their density is fairly high [7]. It was noted by Kozorezov et al. [8] that recombination can give rise to a dependence of the detector's signal amplitude on the coordinate of the site where a photon is absorbed. For example, in the case of photon absorption near the electrode boundary, the spread of the cloud of nonequilibrium quasiparticles occurs somewhat slower than in the case of the photon absorption in the detector's center. As a result, recombination losses are found to be larger in the vicinity of the boundary; it is this circumstance that brings about the inhomogeneous broadening of the detector's line.

The data reported in [9] substantiate the above assumption. Unfortunately, the analysis [9] was complicated since the detectors with two active electrodes in which the effects of multiple tunneling of quasiparticles [10] took place were considered. In these detectors, the quasiparticles are not lost after the first tunneling from the electrode in which the photon was absorbed; rather, they continue to be involved in tunneling in the opposite direction, and also contribute to the signal. In this case, one should take into account the recombination- and edge-related losses for both electrodes whose properties are always different owing to technological conditions.

In this study, we consider the effect of the edge- and recombination-related losses of quasiparticles for the detectors that have a specific design, in which case only one electrode is active, while the properties of the other electrode are suppressed using an additional trapping layer deposited on the side opposite to the tunneling barrier (the passive electrode). In Section 2, we describe the structure of tunneling detectors and experimental methods. In Section 3, we present the experimental spectra and consider their structure; experimental data on the dependence of the detector's signal on the energy of an X-ray photon are also reported. In Section 4, we describe the diffusion model of the detector (this model takes into account the recombination- and edge-related losses of quasiparticles) and report the results of simulations. In Sections 5 and 6, the dependence of the detector's signal on the photon energy and the instrument-related line shape are analyzed on the basis of the diffusion model.

It is worth noting that the detectors with the passive electrode exhibit a number of potential advantages compared to detectors with multiple tunneling. First, it was expected that this structure would make it possible to avoid doubling of lines, typical of STJ detectors with two active electrodes. Second, the contribution of boundary regions to the instrument-related line shape should be reduced owing to the relatively small diffusion length [11].

2. EXPERIMENTAL

The samples of detectors to be studied were fabricated by the method of magnetron sputtering at the Institute of Radio Engineering and Electronics of the Russian Academy of Sciences. The detectors had a multilayered structure, specifically, Ti/Nb(1)/Al(1)/AlO_x/Al(2)/Nb(2)/NbN. The schematic representation of the detector and the energy structure of the quasiparticles' levels are shown in Fig. 1. The bottom electrode that was assumed to be passive consisted of three layers that were deposited sequentially onto the silicon substrate: 30 nm of titanium; 100 nm of niobium, Nb(1); and 8 nm of aluminum, Al(1). The Al_2O_3 barrier layer with the thickness of 1–2 nm was formed as a result of aluminum oxidation. The superconducting gap in the vicinity of the tunneling barrier was governed by the Nb(1) layer and was equal to ~1.4 meV. A considerable decrease in the superconducting gap occurred in the titanium layer. This gap was controlled by the low temperature of the transition to the superconducting state of titanium ($T_c \approx 0.3$ K) and the proximity effect of the neighboring Nb(1) layer [12]. As a result, the Ti layer played the role of a trap for quasiparticles and prevented their tunneling from the bottom electrode.

The top active electrode was deposited onto Al_2O_3 and also consisted of three layers: a 13-nm thick Al(2) layer, a 150-nm thick Nb(2) layer, and a 30-nm thick NbN layer. The main absorbing layer was that of Nb(2) with the superconducting gap $\Delta \approx 1.4$ meV. The Al(2) layer with a narrower gap served as a trap for quasiparticles. This layer provided for the concentration of qua-

siparticles in the vicinity of the tunnel barrier and increased the rate of tunneling [13]. The NbN layer had a wider gap (the temperature of transition to the superconducting state is $T_c \approx 12$ K) and played the role of reflector of quasiparticles from the outer surface of the electrode.

Thus, the electrodes of the tunneling detector featured radically different properties. In the top electrode, nonequilibrium quasiparticles had a high probability of tunneling and a low probability of losses. As a result, the majority of quasiparticles formed in this electrode tunneled through the barrier and formed the detector's signal. In the bottom electrode, nonequilibrium quasiparticles were captured by the titanium trapping layer and could not be involved in tunneling. As a result, absorption of an X-ray photon in the bottom electrode should not bring about the detector-signal formation. It is also worth noting that the effects of multiple tunneling of quasiparticles should be absent in the detectors with the passive electrode [10].

The STJ detectors had the shape of a rhombus with the diagonal ratio 2 : 1 in the plane of layers. Five detectors with the tunneling-barrier areas of 400, 400, 1800, 6400, and 20000 μm^2 were accommodated on a single chip. In order to form separate detectors, we used the methods of photolithography and chemical etching. The dimensions of the bottom electrode exceeded those of the top electrode by ~2 μm. The current-conducting paths were formed of Nb and had the width of 5–10 μm. The method of fabrication of tunneling detectors was described in more detail in [7, 14, 15].

The current–voltage (I–V) characteristics of STJ detectors were measured at temperatures $T = 4.2$–1.35 K. At $T = 4.2$ K, the I–V characteristics of all detectors with various sizes featured the identical shape and differed only in the scale on the current axis. The resistivity of the tunneling barrier amounted to ~3.3 μΩ cm^2. The superconducting gap for the top electrode in the vicinity of the barrier was equal to $\Delta_t = 0.94$ meV and that for the bottom electrode was $\Delta_b = 1.32$ meV.

Tunneling detectors were irradiated using a ^{57}Co radioactive source. The spectrum of this source included five lines: at 6.4 keV (Fe K_α), at 7.04 keV (Fe K_β), and also at 14.4, 122, and 136 keV. The probabilities for radiation to be absorbed in the top electrode were 3.7, 3.1, and 0.42% for the X-ray photons with the energies of 6.4, 7.04, and 14.4 keV, respectively. Harder radiation was practically not absorbed in the detectors' electrodes.

Pulse-height spectra were measured at the samples' temperature $T \approx 1.35$ K. In order to suppress the Josephson current, we applied a magnetic field with the strength as high as 200 Oe; this field was directed parallel to the plane of the tunneling barrier and along the short axis of the rhombus. In the experiment, we used a charge-sensitive preamplifier; the signal at the output of this preamplifier was proportional to the charge transported by the tunneling current. Experimental data were reported previously [16, 17].

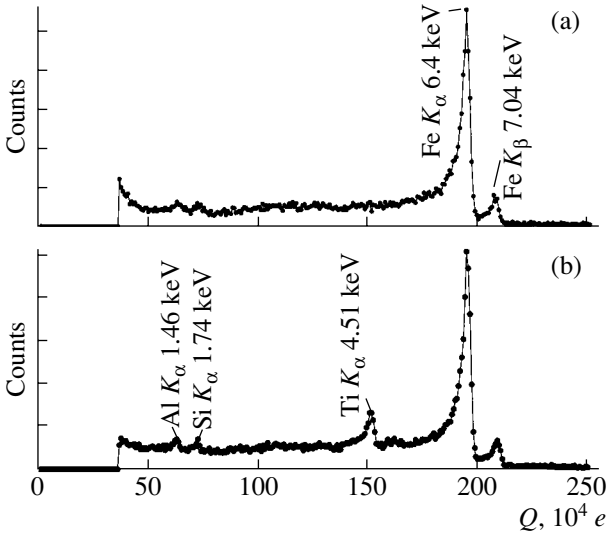

Fig. 2. Pulse-height spectra of an STJ detector with an area of 6400 μm^2. Q is the charge transported by tunneling current. Spectrum (a) was obtained using the ^{57}Co source and spectrum (b) was obtained using the ^{57}Co source with an additional Ti screen.

3. PULSE-HEIGHT SPECTRA OF TUNNELING DETECTORS

In Fig. 2a, we show the pulse-height spectrum obtained in the case of irradiation of a tunneling detector (with an area of 6400 μm^2) with X-ray photons from the ^{57}Co source. Two clearly pronounced lines correspond to absorption of the X-ray photons with energies of 6.4 keV (Fe K_α) and 7.04 keV (Fe K_β) in the detector's top electrode. The width of the line at 6.4 keV (Fe K_α) is equal to ~115 eV with the contribution of electronic noise amounting to 75 eV. The intrinsic energy resolution of the detector is ~90 eV, which is appreciably better compared with the Si- and Ge-based detectors. However, the obtained resolution is much lower than the values expected for this type of STJ detectors ($\Delta E_{\mathrm{Th}} \approx 5$ eV). It is also worth noting that experimental line is asymmetric, with a steep right-hand edge and extended falloff on the side of lower energies. This shape of the line is typical of broadening caused by the dependence of the signal on the coordinate where the X-ray photon was absorbed [5].

In the spectrum under consideration, there is no pronounced line that can be attributed to the photons with the energy of 14.4 keV. Instead, we observe a continuous spectrum that extends from zero values to the amplitudes that exceed the values of the X-ray lines at 6.4 and 7.04 keV. This shape of the spectrum is related to incomplete absorption of the X-ray photons in the detector's electrodes. Indeed, the X-ray photons with

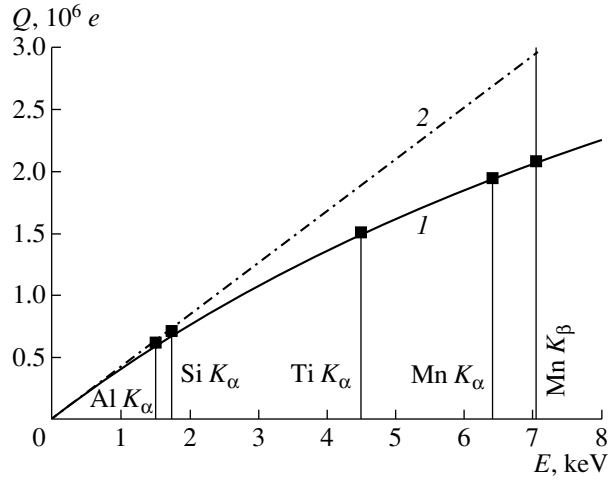

Fig. 3. Calibration of the detector's signal in energies: squares represent experimental data for an STJ detector with an area of 6400 μm^2, curve *1* represents the results of calculations based on the diffusion model, and curve *2* corresponds to the theoretical detector's signal in the absence of recombination.

energies from 2 to 19 keV are absorbed mainly owing to photoeffect at the *L* shell of Nb atoms; the absorption is accompanied by emission of photoelectrons and subsequent Auger electrons. For X-ray photons with an energy of 14.4 keV, a primary photoelectron has an energy of ~11.7 keV and the mean free path of ~550 nm, which is severalfold larger than the electrode's thickness (193 nm). Due to multiple scattering events, there is almost 100% probability of a photoelectron leaving the electrode. As a result, the peak of total absorption is virtually absent, while the continuous signal spectrum corresponds to partial absorption of the photon energy (14.4 keV) caused by the fact that the photoelectron leaves the detector.

For the X-ray photons with an energy of ~6 keV, the primary photoelectrons have a lower energy (~3.2 keV) and a shorter mean free path (~60 nm). The Auger electrons have an energy of ~2 keV and an even shorter mean free path (~24 nm). Thus, the mean free path of these electrons is smaller than the electrode's thickness. Therefore, the spectrum should consist of the total-absorption peak and a continuous spectrum corresponding to the events that occur in the surface layers of electrodes and are accompanied by the escape of photoelectrons. It is noteworthy that a contribution to the continuous spectrum is also made by events where an X-ray photon is absorbed in the bottom electrode but a fraction of the photoelectrons cross the barrier and deposit their energy in the top electrode.

There are no signals that correspond to absorption of X-ray photons in the bottom (passive) electrode in the spectra shown in Fig. 2. These signals have a tenfold smaller amplitude and fall in region of small amplitudes (below the discrimination threshold). The causes of the incomplete suppression of signals related to the passive electrode were considered partially in [11, 14].

In Fig. 2b, we show the spectrum obtained using the same detector; however, a Ti screen was additionally installed in this case. This screen had a cylindrical shape and its axis coincided with the line that connected the ^{57}Co source with the detector. The latter could detect both the source radiation and the characteristic X-ray radiation that originated from Ti and was excited by the source's radiation. An additional line that corresponds to the Ti K_α line with an energy of 4.51 keV can be seen in the spectrum. In addition, there are two small-amplitude peaks in the region of low energies; these peaks can be attributed to the X-ray lines Si K_α with an energy of 1.74 keV and Al K_α with an energy of 1.46 keV; these lines are excited by radiation of the ^{57}Co source in the silicon substrate and aluminum layers of the detector. Thus, five X-ray lines are observed simultaneously in the spectrum, which makes it possible to calibrate the detector signal with respect to energy.

In Fig. 3, we show the detector-signal amplitudes (squares) for various energies of X-ray radiation. A pronounced nonlinearity is observed; this nonlinearity can be naturally related to inherent recombination of nonequilibrium quasiparticles. It is noteworthy that, in contrast to the data in publications [6, 18, 19], where the response nonlinearity was not clearly pronounced, nonlinear recombination-related effects manifest themselves most clearly in detectors with a passive electrode.

4. DIFFUSION MODEL OF A TUNNELING-JUNCTION DETECTOR

The obtained experimental data were analyzed using a mathematical model that takes into account diffusion of quasiparticles in the detector's electrodes. Since the thickness of the electrodes was much smaller than their sizes in the two other dimensions, the problem was considered as two-dimensional. Nonequilibrium quasiparticles are described by the concentration function $u(x, y, t)$, where $\{x, y\}$ are coordinates in the plane of electrodes, and t is time. The function $u(x, y, t)$ satisfies the diffusion equation into which an additional term taking into account the recombination of quasiparticles is introduced; this equation is written as

$$\frac{\partial u}{\partial t} = D\left(\frac{\partial^2 u}{\partial x^2} + \frac{\partial^2 u}{\partial y^2}\right) - \gamma_T u - \gamma_L u - R_{\text{ef}} u^2, \qquad (1)$$

where D is the diffusion coefficient, γ_T and γ_L are the rates of tunneling and loss of quasiparticles, and R_{ef} is the recombination constant [20].

The initial conditions are described by a Gaussian function

$$u(x, y, t = 0) = \frac{N_0}{\pi a_0^2} \exp\left[-\frac{(x - x_0)^2 + (y - y_0)^2}{a_0^2}\right], \quad (2)$$

where N_0 is the number of quasiparticles formed as a result of absorption of an X-ray photon with an energy E ($N_0 = E/1.75\Delta$ [21]), $\{x_0, y_0\}$ are the coordinates of the point where an X-ray photon was absorbed, and a_0 is the size of the initial region.

The boundary conditions are expressed as

$$\frac{\partial u}{\partial n} + \beta u|_\Gamma = 0, \tag{3}$$

where Γ is the boundary of the electrode, $\partial u/\partial n$ is the derivative along the outer normal to the boundary Γ, and β is a parameter proportional to the probability that a quasiparticle is lost at the boundary.

The detector's signal is given by the integral with respect to two-dimensional surface area G of the electrode and time t; i.e.,

$$Q(x_0, y_0) = e\gamma_T \int_0^\infty dt \iint_C u(x, y, t)dxdy, \tag{4}$$

where e is the elementary charge.

The shape of the instrument-related line of the detector is given by

$$s(Q) = \frac{1}{\sqrt{2\pi}A\sigma_0}\iint_G \exp\left(-\frac{[Q - Q(x_0y_0)]^2}{2\sigma_0^2}\right)dx_0dy_0, \tag{5}$$

where A is the electrode's area and σ_0^2 is the variance determined by the inherent and electronic noise factors in the detector [10]. Electronic noise can be assessed from the width of the generator's peak.

Constants in the diffusion Eq. (1) are averaged quantities, with averaging carried out over the energy and electrode thickness. It was shown in [12, 22] that, in multilayer structures, these constants depend on the properties of the materials that form the electrodes, on the microstructure of these materials, and also on the properties of the interfaces between the layers. Therefore, calculation of these constants is a fairly complex problem; the values obtained can depend on the fabrication technology for STJ detectors.

From the practical viewpoint, in order to estimate the quantities that appear in diffusion Eq. (1), it is appropriate to use simpler approximate expressions, while we can try to obtain the actual values from a comparison of experimental data with the results of calculations. In particular, the following expression can be used for the diffusion coefficient [22]:

$$D = \frac{1}{3}v_F l_f \sqrt{\frac{2k_BT}{\pi\Delta}}. \tag{6}$$

Here, v_F is the velocity of electrons at the Fermi surface, l_f is the mean free path of quasiparticles, Δ is the superconducting gap in the proximate Al/Nb layer, and k_B is the Boltzmann constant.

Assuming that l_f is equal to the size of crystallites in the Nb film ($l_f \approx 5$ nm), $v_F(\text{Nb}) = 0.57 \times 10^8$ cm/s, $T = 1.35$ K, and $\Delta = 0.94$ meV, we obtain the value of $D = 2.6$ cm^2/s for the diffusion coefficient.

The effective lifetime of nonequilibrium quasiparticles $\tau_{\text{ef}} = (\gamma_T + \gamma_L)^{-1}$ is approximately equal to the rise time of the detector's signal τ_{RT}. For the spectra shown in Fig. 2, $\tau_{RT} = 0.125$ μs. Therefore, the diffusion length for nonequilibrium quasiparticles $\Lambda_D = \sqrt{D\tau_{\text{ef}}} = 5.6$ μm. Thus, for all detectors (except for those with the smallest area), the sizes of electrodes exceed severalfold the diffusion length.

In order to carry out simulations and compare the results with experimental data, we solved diffusion Eq. (1) with the quadratic recombination-related term by numerical methods using the grid functions [5]. In this case, we calculated the collected charge $Q(x_0, y_0)$ for various coordinates $\{x_0, y_0\}$ that corresponded to the site where an X-ray photon was absorbed; we then calculated the shape of the detector line, in accordance with expression (5).

Typical dependences of the collected charge $Q(x_0, y_0)$ on the coordinate of the site where an X-ray photon was absorbed are shown in Fig. 4a. The coordinates $\{x_0, y_0\}$ along the short diagonal of the rhombus are depicted along the positive X semiaxis. Coordinates along the section that connects the rhombus center with the middle of the side face are plotted on the negative X semiaxis. In Fig. 4b, we show the corresponding instrument-related lines. Calculations were carried out for the X-ray photons with an energy of 6.4 keV that were detected by an STJ detector with an area of 1600 μm^2. The diffusion length Λ_D was equal to 4.5 μm, and the probability of tunneling amounted to $P_1 = \gamma_T/(\gamma_T + \gamma_L) = 0.75$.

Curve *1* in Fig. 4a corresponds to the case where the edge losses are in effect ($\beta = 0.036$ μm^{-1}), while there is no recombination ($R_{\text{ef}} = 0$). If the diffusion length is small, absorption of an X-ray photon at the electrode center ($x_0 = y_0 = 0$) yields the collected charge $Q_D = N_0P_1$. The edge losses reduce the charge Q only in the peripheral regions. It is noteworthy that the signal Q is smaller in the electrode corners than in the middle of the faces.

Curve *2* in Fig. 4 corresponds to the case where edge losses are absent ($\beta = 0$) but recombination losses are present, $R^*_{\text{ef}} = 2.02 \times 10^{-5}$ μm^2, where $R^*_{\text{ef}} = R_{\text{ef}}\tau_{\text{ef}}$. A noticeable decrease in the signal is observed both in the central and peripheral regions of the electrode. Additional attenuation of the signal Q in the vicinity of the corners and sides of the electrode is caused by the slower spreading of nonequilibrium quasiparticles in these regions and, correspondingly, by larger recombination-related losses.

Curve *3* is caused by the combined effect of the recombination- and edge-related losses. The signal at

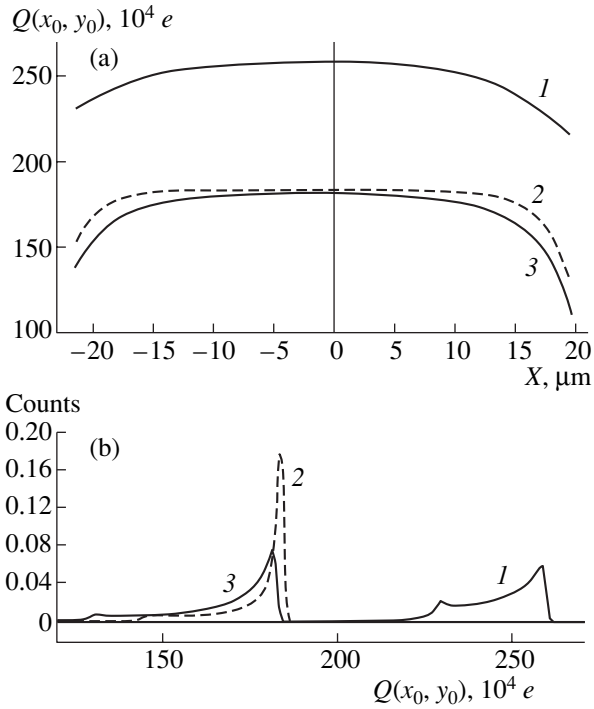

Fig. 4. (a) Dependence of the STJ-detector signal Q on the coordinate of the point onto which the X-ray photon was incident (calculation based on the diffusion model). The positive X semiaxis represents the coordinates $\{x_0, y_0\}$ along the short diagonal of the rhombus, while the negative X semiaxis represents the coordinates along the line that connects the rhombus' center with the middle of the side. The following values of the parameters were used in the calculation: (*1*) $R_{ef} = 0$ and $\beta = 0.036$ μm^{-1}; (*2*) $R^*_{ef} = 2.02 \times 10^{-5}$ μm^2 and $\beta = 0$; and (*3*) $R^*_{ef} = 2.02 \times 10^{-5}$ μm^2 and $\beta = 0.036$ μm^{-1}. (b) Detector lines *1*, *2*, and *3* correspond to the curves *1*, *2*, and *3* in panel (a).

the detector's center is attenuated by recombination, while it is attenuated by both the recombination- and edge-related losses in the vicinity of the boundaries. It is worth noting that, as calculations show, the contributions of the edge- and recombination-related losses are not additive. It can be seen from Fig. 4b that, in this case, an additional broadening of the instrument-related detector's line occurs, and a "tail" extending to the region of small amplitudes is formed. It is this case that corresponds to the experimental data reported in this communication.

5. DEPENDENCE OF STJ-DETECTOR SIGNAL ON THE ENERGY OF THE X-RAY PHOTON

The diffusion model with the recombination-related term was used to analyze the dependence of the detector's signal on the energy of absorbed X-ray photon. The experimental data (squares in Fig. 3) correspond to the absorption of X-ray photons in the electrode's center; therefore, the edge-related losses can be disregarded. The following three parameters were varied in the course of calculations: the tunneling probability P_1, diffusion length Λ_D, and recombination parameter R^*_{ef}. The size of the initial region was assumed to be equal to $a_0 = 1$ μm [9].

Curve *1* in Fig. 3 represents the result of calculation and was obtained by adjusting the parameters mentioned above. The tangent to the calculated curve at the point $E = 0$ (straight line *2*) determines the value of the parameter $P_1 = 0.775$. In the case where there is no recombination, the detector's signal should depend linearly on the energy of the X-ray photon and vary along this line as

$$Q_0(E)\big|_{R^*_{ef} = 0} = \frac{E}{1.75\Delta}P_1. \quad (7)$$

It can be seen from Fig. 3 that, at energies in excess of 2 keV, recombination-related losses bring about a noticeable attenuation of the signal; this attenuation amounts to ~30% even at $E = 7$ keV. This means that recombination should also give rise to an appreciable broadening of the detector line.

The parameters Λ_D and R^*_{ef} cannot be determined unambiguously from the dependence $Q(E)$. In the first approximation, the recombination-related losses are given by the following expression [7]:

$$\Delta Q_R \approx \frac{N_0^2 R^*_{ef}}{4\pi\Lambda_D^2}\ln\frac{\Lambda_D}{a_0}. \quad (8)$$

It can be seen from formula (8) that the recombination-induced attenuation of the signal at the electrode's center depends first of all on the ratio R^*_{ef}/Λ_D^2, which is equal to ~10^{-6} in the case under consideration.

6. SHAPE OF THE LINE OF TUNNELING DETECTORS

In the next stage, the diffusion model was used to analyze the shape of the line of tunneling detectors. As experimental data, we used simpler spectra obtained in the case of irradiation with X-ray photons from the ^{55}Fe radioactive source that involved only two lines: at 5.9 keV (Mn K_α) and at 6.4 keV (Mn K_β). Experimental spectra included, in addition to the lines corresponding to the total absorption of X-ray photons K_α and K_β, also a continuous spectrum that corresponds to the escape of photoelectrons from surface layers (see Section 3). The fraction of these events is independent of the electrodes' area and is not described by the diffusion model. In this context, the continuous spectrum was approximated by a straight line and was subtracted from the total spectrum.

In Figs. 5a and 5b, we show the spectra of instrument-related lines that correspond to the absorption of

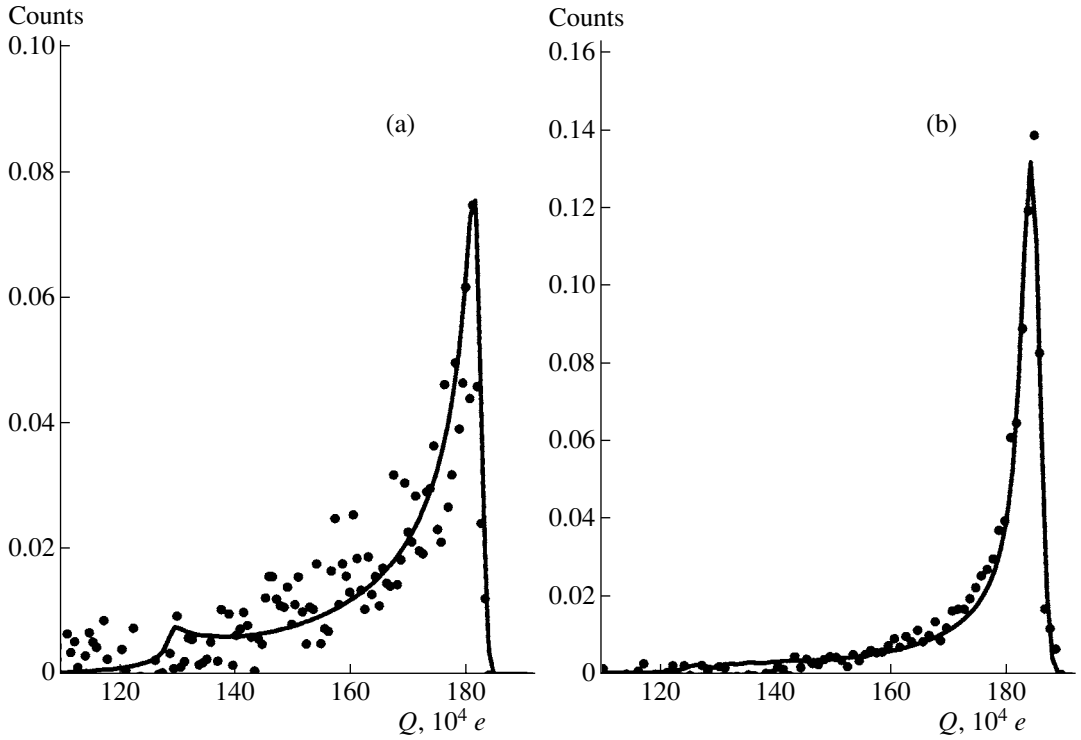

Fig. 5. Spectra of STJ detectors for the 5.9-keV X-ray line. The detector's area is (a) 1600 and (b) 6400 μm^2. The circles correspond to experimental data and the solid curves represent the results of calculations based on the diffusion model and fitted to experimental data.

5.9-keV X-ray photons for detectors with the areas of 1600 and 6400 μm^2. It can be seen from Fig. 5 that the lines are narrowed as the area of the STJ detector is increased. Such change in the spectra is caused by a decrease in the contribution of the interfacial region to the total spectrum.

In the calculations based on the diffusion model, we varied the following three parameters: the diffusion length Λ_D, recombination parameter R^*_{ef}, and the edge-loss parameter β. The probability of tunneling P_1 was assumed to be equal to the value obtained as a result of analysis of the signal's dependence on the energy of X-ray photons ($P_1 = 0.775$). Adjustment of the parameters was carried out so that satisfactory agreement was attained simultaneously for tunneling detectors of all sizes. Such an approach is quite justified since all detectors were formed on the same chip, were fabricated simultaneously, and should have identical physical parameters.

The calculated curves providing the best fit to the experimental data are shown in Fig. 5 by solid curves. It can be seen that the diffusion model adequately describes the main features of the spectra. We used the following values of the parameters in the calculations: $\Lambda_D = 4.5$ μm, $\beta = 0.036$ μm^{-1}, and $R^*_{\text{ef}} = 2.2 \times 10^{-5}$ μm^2. The value of the diffusion length Λ_D is consistent with estimates based on formula (6). The edge-loss parameter β has a value that is typical of the detectors fabricated using the technology under consideration [23]. It is worth noting that our calculations show that both factors (recombination- and edge-related losses of quasiparticles) affect the width of the detector's line.

The recombination constant obtained in this study can be compared with the data reported in [9] (R^*_{Top} = 4–5 μm^3 s^{-1}). In our calculations, we obtained the recombination constant R^*_{ef} for the two-dimensional case; this constant is related to the 3D constant R^*_3 by the expression

$$R^*_3 = R^*_{\text{ef}} d_{\text{ef}}/\tau_{\text{ef}}, \quad (9)$$

where d_{ef} is the thickness of the proximate Al/Nb layer in which motion of nonequilibrium quasiparticles occurs. Using for d_{ef} the value $d_{\text{ef}} \approx d(\text{Al}) + 2\xi(\text{Nb}) \approx$ 43 nm, where ξ(Nb) is the coherence length in the Nb film, we obtain the value of $R^*_3 \approx 6.9$ μm^3 s^{-1} for the recombination constant; this value is somewhat larger than that reported in [9]. However, taking into account differences in the fabrication of STJ detectors and in the thickness of Al/Nb layers and their microstructure, we believe that the obtained value of R^*_3 indicates rather that the parameters are in agreement.

Thus, the diffusion model makes it possible to describe the line shape for the STJ detectors and yields acceptable values for all adjustable parameters.

7. CONCLUSIONS

The effect of the recombination- and edge-related losses of quasiparticles on the detection parameters manifests itself most clearly in the developed STJ detectors with a passive electrode. The diffusion model makes it possible to correctly describe the shape of the line in the tunneling detectors and calculate the dependence of the signal on the energy of the X-ray photon.

Our studies show that recombination of quasiparticles can appreciably affect the operation of the tunneling detectors. Recombination-related losses give rise to nonlinearity of the detector's signal in relation to the energy of absorbed X-ray photons, reduce the signal amplitude, and bring about broadening of the detector's line.

The intensity of recombination-related losses is governed by the ratio between the recombination constant and the squared diffusion length. As a result, the recombination-related effects are most pronounced in the detectors with a fine-crystalline structure of electrodes, where the diffusion rate for quasiparticles is low.

The second factor affecting the recombination efficiency is the rate of escape of 2Δ phonons. In the detectors with a passive electrode, the 2Δ phonons are absorbed in the Ti trapping layer, which brings about both an enhancement of recombination and the most clearly pronounced nonlinear effects. In the detectors with two active electrodes, the escape of the 2Δ phonons brings about a redistribution of quasiparticles between the detector's electrodes (a phonon exchange) [7]. In this case, the recombination-related effects are suppressed.

In order to reduce the role of recombination-related processes, one should use epitaxial films for the detector's electrodes or develop structures that could make it possible to compensate losses of quasiparticles in the interfacial regions of the electrodes.

ACKNOWLEDGMENTS

We thank M.G. Kozin and I.L. Romashkina for their help with preparation of instrumentation and samples.

REFERENCES

1. N. E. Booth and D. J. Goldie, Supercond. Sci. Technol. **9**, 493 (1996).
2. V. S. Shpinel', V. A. Andrianov, and M. G. Kozin, Izv. Ross. Akad. Nauk, Ser. Fiz. **59** (11), 2 (1995).
3. *Proceedings of 10th International Workshop of Low Temperature Detectors, LTD-10, Genoa, Italy, 2003*, Ed. by F. Gatti, Nucl. Instrum. Methods Phys. Res. A **520** (2004).
4. O. J. Luiten, M. L. Van den Berg, J. Gomez Rivas, et al., in *Proceedings of 7th International Workshop of Low Temperature Detectors, LTD-7*, Ed. by S. Cooper (Munich, Germany, 1997), p. 25.
5. V. A. Andrianov and V. P. Gor'kov, Prikl. Mat. Inf., No. 19, 5 (2004).
6. P. Verhoeve, N. Rando, J. Verveer, et al., Phys. Rev. B **53**, 809 (1995).
7. V. A. Andrianov, V. P. Gor'kov, M. G. Kozin, et al., Fiz. Tverd. Tela (St. Petersburg) **41**, 1168 (1999) [Phys. Solid State **41**, 1063 (1999)].
8. A. G. Kozorezov, J. K. Wigmore, R. den Hartog, et al., Phys. Rev. B **66**, 094510 (2002).
9. R. den Hertog, A. G. Kozorezov, J. K. Wigmore, et al., Phys. Rev. B **66**, 094511 (2002).
10. D. J. Goldie, P. L. Brink, C. Patel, et al., Appl. Phys. Lett. **64**, 3169 (1994).
11. V. A. Andrianov, P. N. Dmitriev, V. P. Koshelets, et al., AIP Conf. Proc. **605**, 165 (2002).
12. A. A. Golubov, E. P. Houwman, J. G. Gijsbertsen, et al., Phys. Rev. B **51**, 1073 (1995).
13. N. E. Booth, Appl. Phys. Lett. **50**, 293 (1987).
14. M. G. Kozin, I. L. Romashkina, S. A. Sergeev, et al., Nucl. Instrum. Methods Phys. Res. A **520**, 250 (2004).
15. V. A. Andrianov, M. G. Kozin, S. A. Sergeev, et al., Fiz. Nizk. Temp. **23**, 1187 (1997) [Low Temp. Phys. **23**, 889 (1997)].
16. V. A. Andrianov, L. V. Filippenko, V. P. Koshelets, and M. G. Kozin, in *Abstracts of the LV National Conference of Nuclear Physics: Frontiers in Physics of Nucleus* (St. Petersburg, 2005), p. 316.
17. V. A. Andrianov, M. G. Kozin, I. L. Romashkina, et al., in *Abstracts of the LV National Conference of Nuclear Physics: Frontiers in Physics of Nucleus* (St. Petersburg, 2005), p. 329.
18. N. Rando, A. Peacock, A. van Dordrecht, et al., J. Appl. Phys. **76**, 2490 (1994).
19. S. E. Labov, L. H. Hiller, C. A. Mears, et al., IEEE Trans. Appl. Supercond. **5**, 3034 (1995).
20. S. B. Kaplan, C. C. Chi, D. N. Langenberg, et al., Phys. Rev. B **14**, 4854 (1976).
21. N. Rando, A. Peacock, A. van Dordrecht, et al., Nucl. Instrum. Methods Phys. Res. A **313**, 173 (1992).
22. B. Ivlev, G. Pepe, and U. Scotti di Uccio, Nucl. Instrum. Methods Phys. Res. A **300**, 127 (1991).
23. V. A. Andrianov and V. P. Gorkov, AIP Conf. Proc. **605**, 39 (2002).

Translated by A. Spitsyn